Neuron
Report

Neuronal Selectivity and Local Map Structure in Visual Cortex

Ian Nauhaus,[1] Andrea Benucci,[2] Matteo Carandini,[2] and Dario L. Ringach[3,4,*]
[1]Biomedical Engineering Department, University of California, Los Angeles, CA 90095, USA
[2]Smith-Kettlewell Eye Institute, San Francisco, CA 94115, USA
[3]Neurobiology Department
[4]Psychology Department
Jules Stein Eye Research Institute, David Geffen School of Medicine, University of California, Los Angeles, CA 90095, USA
*Correspondence: dario@ucla.edu
DOI 10.1016/j.neuron.2008.01.020

SUMMARY

The organization of primary visual cortex (V1) into functional maps makes individual cells operate in a variety of contexts. For instance, some neurons lie in regions of fairly homogeneous orientation preference (iso-orientation domains), while others lie in regions with a variety of preferences (e.g., pinwheel centers). We asked whether this diversity in local map structure correlates with the degree of selectivity of spike responses. We used a combination of imaging and electrophysiology to reveal that neurons in regions of homogeneous orientation preference have much sharper tuning. Moreover, in both monkeys and cats, a common principle links the structure of the orientation map, on the spatial scale of dendritic integration, to the degree of selectivity of individual cells. We conclude that neural computation is not invariant across the cortical surface. This finding must factor into future theories of receptive field wiring and map development.

INTRODUCTION

Neurons in primary visual cortex (V1) exhibit large heterogeneity in their receptive field properties (Schiller et al., 1976; De Valois et al., 1982; Ringach et al., 2002). Explaining the origin of such diversity could shed light on the microcircuitry generating V1 receptive fields. One hypothesis is that a neuron's tuning properties are correlated with the local structure of functional maps in its neighborhood (Callaway, 1998; Ferster and Miller, 2000; McLaughlin et al., 2003; Schummers et al., 2004; Sompolinsky and Shapley, 1997). The diversity of tuning properties could then result from the corresponding heterogeneity in local map structure. For example, if one models a neuron's response as arising in part from the spatially symmetric pooling of local activity, there is a predicted dependence of orientation tuning bandwidth on the neuron's location within the orientation map. Indeed, this dependence has been observed for the subthreshold responses (Marino et al., 2005; Schummers et al., 2002). On the other hand, a number of studies failed to find this dependence in the spike responses (Maldonado et al., 1997; Marino et al., 2005; Schummers et al., 2002), suggesting that neural computation is invariant across the cortical surface.

Here, we studied the relationship between orientation bandwidth in spike responses and the local structure of the orientation map. Our method is based on a combination of optical imaging (Blasdel, 1992; Bonhoeffer and Grinvald, 1991, 1993) and multielectrode array recordings that provides an accurate localization of electrodes within a map of orientation preference (Nauhaus and Ringach, 2007). In both cats and in monkeys, we found that neurons are more sharply tuned for orientation in regions of homogeneous orientation preference (iso-orientation domains) than in heterogeneous regions of the map (e.g., near pinwheel centers). Furthermore, we demonstrate that a single principle links neuronal selectivity and the local map structure in both species. This principle connects two hitherto disjoint observations: that neurons are more selective for orientation in cat than in monkey, and that orientation preference maps have finer scale in monkey than in cat. Our findings indicate that the heterogeneity in receptive field properties of cortical cells, such as orientation bandwidth (Schiller et al., 1976; De Valois et al., 1982; Ringach et al., 2002), is partially explained by the location of neurons within functional maps.

RESULTS

The technique that we used involves measuring the orientation map with optical means and then recording from multiple neurons with an electrode array. As a first step, we obtained the orientation map on a cortical patch of V1 using optical imaging (Bonhoeffer and Grinvald, 1991; Grinvald and Hildesheim, 2004) (Figure 1A). Subsequent to the acquisition of the orientation maps, we implanted a 10 × 10 electrode array with grid spacing of 400 μm on the same area that was imaged. We then measured the orientation tuning of neuronal responses across the array using reverse correlation in the orientation domain, where the stimulus consists of a rapid sequence of gratings at random orientation (Ringach et al., 1997). The average orientation-triggered response, at the optimal time delay, generates an orientation tuning curve (Figure 1B). A Gaussian fit to each tuning curve provides an estimate of the preferred orientation, θ_O, and tuning width, $\Delta\theta$ (Figure 1B). This dynamic measurement of orientation selectivity yields results that correlate very

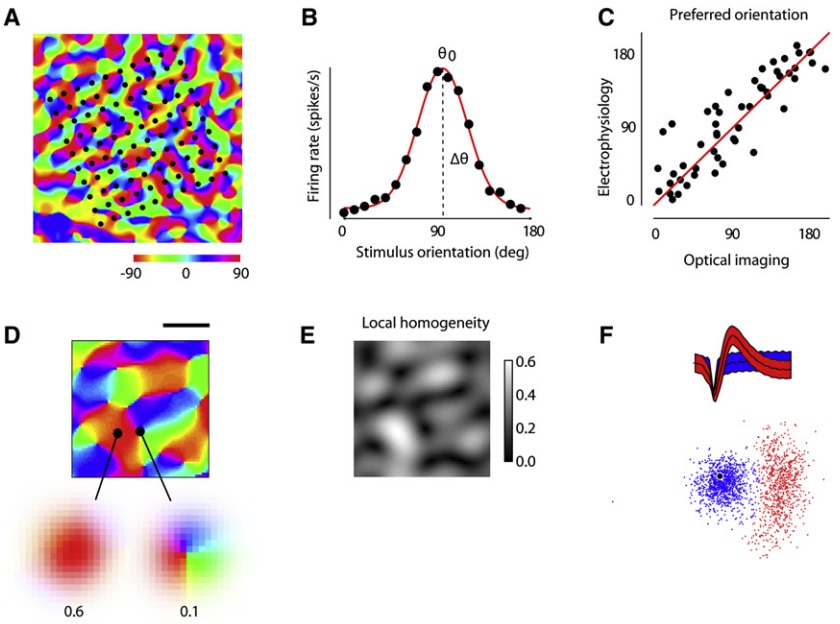

Figure 1. Recording Receptive Field Properties across Functional Maps of Cortex

(A) Optical imaging was used to measure the orientation maps in cats and monkeys. An example of a measurement in monkey is shown here.

(B) A rapid sequence of gratings of pseudorandom orientation was used to stimulate all cells in the array. This yields a tuning curve for each electrode, resulting from the stimulus-triggered averages of the responses (solid dots). The tuning curve is then fit with a Gaussian (red curve) to yield an estimate of preferred orientation (θ_0) and tuning width ($\Delta\theta$).

(C) The location of the array is estimated by finding the placement that produces maximal agreement between the optical and electrophysiological estimates of preferred orientation (Nauhaus and Ringach, 2007). The scatterplot shows the best correlation between these two variables in one of the experiments. The estimated location of the array is shown by the black dots in (A).

(D) Detail of the orientation preference map, with the local homogeneity index computed for two pixels: one in an iso-orientation domain (where the index is 0.6) and one near a pinwheel center (where the index is 0.1).

(E) A map of the local homogeneity index for the same patch of cortex.

(F) Isolation of single units. In the scatterplot each dot represents a waveform that has crossed threshold for the example electrode. The x axis and y axis are the first and second principal coefficients of the waveforms. The blue cloud near the origin of the graph (black dot) is the noise and the red dots are spikes. The corresponding average waveforms for each cloud, ± 1 standard deviation, are shown on top.

well with those obtained in both simple and complex cells using drifting-grating stimuli (Nishimoto et al., 2005).

To estimate the position of the array with respect to the orientation map, we searched for the location that yields the maximum agreement between the preferred orientations measured optically and those measured from the electrode array. The outcome of this computation in one experiment is shown in the scatterplot of Figure 1C, along with the estimated location of the array in Figure 1A. The location of the array on the surface of the cortex is determined by just three parameters: two for its translation and one for its rotation. Because the number of parameters is small compared with the number of electrodes, the optimization problem is greatly overdetermined and robust to noise. The correlation between preferred orientations measured optically and electrically drops off rapidly as the array is misplaced from its actual location (Nauhaus and Ringach, 2007). The technique yields average localization errors of only ~30 μm, i.e., on the scale of a single cell body. As we discuss below, this accurate localization of the electrodes is essential for the purposes of this study.

Once the array location was estimated, we computed a measure of homogeneity in orientation preference for the neighborhood surrounding each electrode. We define a *local homogeneity index* at a cortical point by computing the magnitude of a vector sum. The vector angles are determined by the orientations in the map, and the magnitudes are defined by a spatial 2D Gaussian window centered at the given cortical point (see Experimental Procedures). The standard deviation of the Gaussian, σ, defines the spatial scale of analysis around each point. We chose σ = 180 μm to approximate the dendritic field size of superficial layer neurons in both cats (Gilbert and Wiesel, 1979; Hirsch, 2003; Marino et al., 2005) and monkeys (Callaway, 1998; Lund and Wu, 1997; Lund and Yoshioka, 1991). The local homogeneity index is bounded between zero and one. It is high in regions that exhibit similar preferences for orientation, such as iso-orientation domains, and low in regions where the preferences for orientation are diverse, such as near pinwheel centers (Figures 1D and 1E).

In the analysis of orientation selectivity versus map structure, we used only carefully isolated single units (Figure 1F). To sort spikes at each electrode, all waveforms that cross threshold were projected onto the principal components. From these data we computed a measure of discriminability (d') between spikes and background, and we found this value to be consistently high (on average, 5.7 ± 1.2), indicating excellent isolation (on average, a hit rate of 99.7% and a false positive rate of 0.2%). Full methods for spike isolation, together with numerous examples, are provided in the Supplemental Data available online.

The relationship between neuronal tuning and local map structure can be studied by relating the tuning width for each electrode yielding single-unit responses to the homogeneity index at that location. Visual examination of the orientation tuning curves and their location within the orientation map in one monkey (Figure 2A) and one cat (Figure 2B) suggests that sharply tuned cells are more frequently present in regions of high homogeneity, while broader tuning is seen near regions of rapid orientation change. This first impression is confirmed by the finding that orientation tuning width and homogeneity index are negatively correlated in both monkeys ($r = -0.56$, $p = 0.00001$, Figure 3A) and cats ($r = -0.56$, $p = 0.00005$, Figure 3B).

The data from the two species were in such good agreement that when the points are superimposed on the same graph,

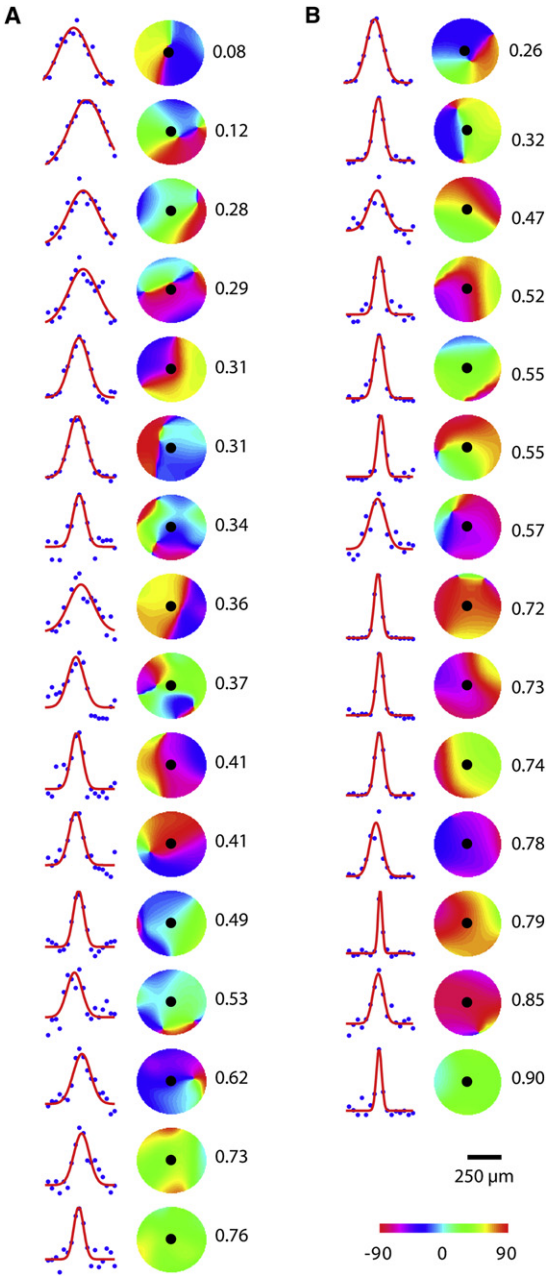

Figure 2. Sharpness of Tuning as a Function of Map Location

Examples of orientation tuning curves and their location within the orientation map are shown for a monkey (A) and a cat (B). All cells obtained in these experiments are shown. They are ranked in order of increasing values of the local homogeneity index (shown near each local orientation map). It appears evident that tuning width decreases with increasing values of the local homogeneity index.

they fall along a single line and are strongly correlated ($r = -0.69$, $p < 10^{-14}$, Figure 3C). This relationship implies that given only the distribution of preferred orientations in the local environment of a V1 neuron, one can use a single rule to predict with high accuracy the neuron's orientation tuning width, regardless of whether it resides in a cat or a monkey. For example, a cell in a cortical site with homogeneity index of 0.5 will have a tuning width of ~20°, independent of the species (Figure 3C).

The common dependence of tuning width on map homogeneity seen in cats and monkeys provides an explanatory link between two hitherto disconnected observations. The first observation is that orientation maps have finer scale in monkeys (Blasdel and Salama, 1986) than in cats (Bonhoeffer and Grinvald, 1991). The second observation is that neurons have sharper tuning in cats than in monkeys (De Valois et al., 1982), with tuning half-width at half-height of ~24° in monkey and ~15° in cat (Ringach et al., 2002; Schiller et al., 1976; Rose and Blakemore, 1974). Our results not only confirm these observations (e.g., compare the maps in Figure 3, and compare the tuning curves in Figure 2), but also predict that one should follow from the other. Because of the difference in spatial scale of the orientation maps in the two species, the local homogeneity index defined at a common scale of analysis (σ = 180 μm) is higher in cat than monkey (Figure 3D). This difference in homogeneity explains the different distributions of tuning width in the two species (Figures 3C and 3E): the prevalence of iso-orientation domains in the cat correlates with the sharper tuning of its neurons. This reasoning is also consistent with the broader tuning for orientation in species lacking orientation maps (Metin et al., 1988; Ohki et al., 2005; Van Hooser et al., 2005; Van Hooser, 2007); we would expect data from these species to lie on the top left of the scatterplot in Figure 3C.

DISCUSSION

The finding of a strong statistical dependence between neuronal selectivity and local map structure is consistent with some previous observations. Tetrode recordings in cat indicate a correlation between the local scatter of preferred orientations and the orientation tuning width of nearby cells (Hetherington and Swindale, 1999). Our findings are consistent with this result because the orientation preference map is highly ordered, even at the finest scale (Ohki et al., 2006), suggesting that an electrode would see a high scatter in orientation preferences only in regions of the map with low homogeneity. Our results also agree with studies that noted a broader orientation tuning near the pinwheels in kittens of 21–34 days of age, and proposed that this effect represents a transient stage of development (Crair et al., 1997; Ohki et al., 2006). Our present results demonstrate that a strong relationship also exists in the adult visual cortex. Finally, our results are consistent with recent intracellular measurements of subthreshold membrane potential responses in cat, whose tuning width was found to be broader near pinwheels than in iso-orientation domains (Marino et al., 2005; Schummers et al., 2002).

Broadening of orientation tuning near singularities has also been suggested based on imaging of intrinsic signals (Swindale et al., 2003). With these signals this trend could arise from light scatter and optical blur, but simulations suggest a remaining effect that could be due to the tuning of individual neurons. Our measurements directly confirm this suggestion.

On the other hand, our results contradict recent studies that reported invariant tuning of spike responses across the orientation map (Marino et al., 2005; Schummers et al., 2002). One possibility for this discrepancy is the coarse sampling of the

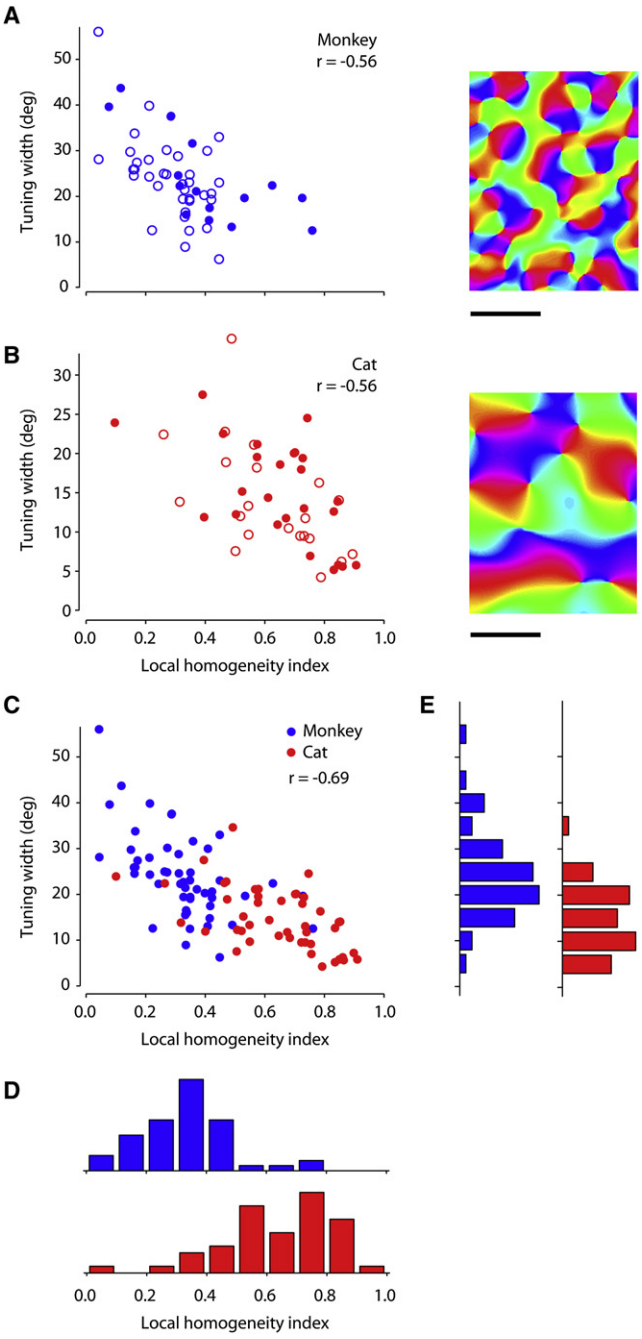

Figure 3. Correlation between Tuning Width and Local Homogeneity Index

Scatterplot of orientation tuning width and local homogeneity index in two monkeys (A) and two cats (B). In both panels, the solid and open symbols correspond to data from two different animals. Correlation between tuning width and local map homogeneity was statistically significant in all individual experiments ($p < 0.01$ in all cases). Typical orientation maps in cat and monkey illustrate the difference in spatial scale between two species (scale bar = 1 mm). (C) A single relationship accounts for data in both species. Data for the two species are plotted together, showing that the points fall on a single line. (D) Marginal distributions of the local homogeneity index for the neurons recorded in the two monkeys (blue, n = 52) and in the two cats (red, n = 46). The mean local homogeneity index is higher in cats (0.64) than in monkeys (0.32), leading to significantly different distributions (rank sum, $p < 10^{-11}$). (E) There is also a pronounced difference between the two species in the orientation selectivity of single cells. The mean σ parameter of a fitted Gaussian function is higher in monkeys (24.0°) than cats (14.6°), again leading to a significant difference between the two species (rank sum, $p < 10^{-6}$).

orientation tuning curves at 22.5° steps used in these investigations. Given the range of tuning widths seen in cat ($\Delta\theta$ = 5°–20°, Figure 3B), this sampling interval rarely allows more than one orientation to be effective in driving any given cell. The consequence is a ceiling effect, as orientation selectivity indices cluster against the upper limit of one (see Figures 1B and 1F and Figure 3D in Marino et al., 2005). This ceiling effect is specific to the firing rate responses; membrane potentials have broader tuning and would not be affected.

The present findings also disagree with a pioneering study (Maldonado et al., 1997) that used intrinsic optical imaging along with targeted tetrode recordings and failed to find a difference in orientation tuning width between cells in pinwheels and iso-orientation domains. The ability to target the desired map locations was supported by a statistical difference in the scatter of preferred orientations between penetrations targeted at pinwheels and others targeted at iso-orientation domains. A closer inspection of these data, however, reveals that penetrations aimed at pinwheels often yielded orientation scatter values comparable to those in iso-orientation domains (compare Figure 3A and 3B in Maldonado et al., 1997). Given that orientation scatter should depend on map location (see above), these effects suggest potential errors in targeting. Indeed, simulations based on our data from the cat show that targeting errors of ~115 μm are sufficient to render the relationship between orientation tuning width and the local homogeneity index undetectable (Figure 4). Achieving such a high precision of visual targeting can be impaired by parallax errors from the reference vasculature and nonnormal electrode penetrations (Nauhaus and Ringach, 2007).

The relationship between bandwidth and map structure that we have uncovered is likely to be even stronger than it appears from our data. Even with relatively accurate electrode localization, we cannot assume that the neurons recorded lie exactly at the location of the electrodes. Their somas might lie some distance away, which contributes to measurement noise in our method. The estimates of the degradation in Figure 4 cannot include such errors. That is, the figure shows how the degradation would occur by adding localization noise above and beyond what is already present in our alignment technique. Therefore, our findings represent a lower bound on the correlation between the bandwidth and the local homogeneity index.

A possible interpretation for the dependence of bandwidth on map structure is that the properties of neurons in the local environment are a critical determinant of orientation selectivity (Marino et al., 2005; McLaughlin et al., 2003; Schummers et al., 2002, 2004). For example, a model in which neurons receive unbalanced excitation and inhibition from an isotropic region around them may account for this effect (Marino et al., 2005). A more detailed model of monkey V1 predicts the observed relationship for complex cells, while predicting the opposite effect for simple cells (McLaughlin et al., 2003). We are unable to test this prediction because the vast majority of our cells are complex (in layers

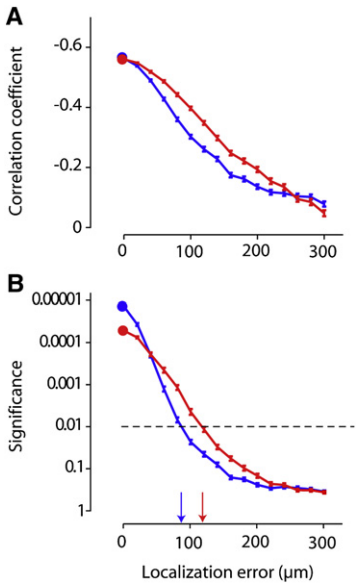

Figure 4. Small Errors in the Localization of the Electrodes Would Obscure the Relationship between Tuning Width and Local Homogeneity Index

For each of our experiments, we ran 200 simulations by independently perturbing each of the estimated electrode locations with Gaussian noise and recomputed the correlation coefficient. (A) Correlation coefficient as a function of the standard deviation of the Gaussian noise. (B) The corresponding statistical significance (p value). The solid dots at zero represent the values achieved by our data without any additional noise. For the monkey data (blue), an artificial displacement of ~80 μm (blue arrow) is sufficient to obscure the relationship between tuning width and local homogeneity index, as statistical significance rises above the 0.01 level. For the cat data (red), the relationship is lost at a displacement of ~115 μm (red arrow). Error bars = SEM.

2 and 3), as determined by the relative magnitude of phase modulation to the dynamic grating sequence (Nishimoto et al., 2005).

There is, however, another interpretation of our findings: the dependent variables (tuning width and local homogeneity index) might be correlated because they are determined by a common factor. For example, a recent theoretical study predicts that tuning should be broader near pinwheels than in iso-orientation domains (Ringach, 2007) based purely on a feedforward connectivity scheme (Alonso et al., 2001; Ferster and Miller, 2000).

The two possible explanations, based on lateral interactions and on feedforward mechanisms, are not mutually exclusive and could each contribute to the generation of the observed relationship. To establish causality and to distinguish between these contributions, future experiments could seek to alter temporarily the local structure of the maps (e.g., pharmacologically; Crook et al., 1991) and study the effects of this alteration on the tuning width of nearby neurons.

It is possible that orientation bandwidth may also be related to other aspects of the V1 functional architecture, such as the location of cytochrome-oxidase patches, ocular dominance domains, or both. We currently lack the data to examine this issue, but our methods are well suited to explore these relationships in future investigations. Maps for stimulus preferences and the degree of selectivity of individual neurons are likely to be intertwined from early on in development (Crair et al., 1997; Ohki et al., 2006). Investigating what other receptive field properties correlate with the local structure of functional maps (such as spatial frequency selectivity, color selectivity, and contrast sensitivity) will help us elucidate the common developmental processes that participate in the early wiring of receptive fields and cortical maps in different species.

EXPERIMENTAL PROCEDURES

Animal Preparation

The data reported here were obtained in two cats and two monkeys. In one cat we recorded in both the right and left hemispheres; thus, there are a total of five data sets.

Experiments were approved by the Institutional Animal Care and Use Committees of the Smith-Kettlewell Eye Research Institute (for cat experiments) and of the Chancellor's Animal Research Committee at UCLA (for monkey experiments), and conducted according to the Guidelines for the Care and Use of Mammals in Neuroscience and Behavioral Research from the National Institutes of Health.

Young adult monkeys (*M. fascicularis,* 3.2–4.2 kg) were sedated with acepromazine (30–60 μg/kg), and anesthetized with ketamine (5–20 mg/kg i.m.) and then with isofluorane (1.5%–2.5%). An endotracheal tube was inserted to allow artificial respiration. All surgical sites were infused with local anesthetic (xylocaine 2%, subcutaneous). After this initial surgery the anesthesia was switched to a combination of sufentanil (0.05–0.2 μg/kg/hr) and propofol (2–6 mg/kg/hr). Young adult cats (2–4 kg) were anesthetized first with ketamine (22 mg/kg i.m.) and Xylazine (1.1 mg/kg i.m.), and then with sodium penthotal (0.5–2 mg/kg/hr i.v.) and fentanyl (typically 10 μg/kg/hr i.v.), supplemented with inhalation of N_2O (typically 70:30 with O_2).

Pupils were dilated with ophthalmic atropine and gas-permeable contact lenses were fitted to protect the corneas. In cats, the nictitating membranes were retracted with topical phenylephrine. Eye movements were prevented by a neuromuscular blocker (pancuronium bromide, 0.10 mg/kg/hr in monkeys, 0.15 mg/kg/hr in cats) administered after surgical procedures were complete.

To ensure a proper level of anesthesia throughout the duration of the experiment, rectal temperature, heart rate, end-tidal CO_2, lung pressure, and EEG were continuously monitored (via a neonatal monitor in monkeys, and a veterinary monitor in cats). In monkeys, we additionally measured noninvasive blood pressure, urine output, and specific gravity (every 4–5 hr to ensure adequate hydration). Drugs were administered in balanced physiological solution at a rate to maintain a fluid volume of 5–10 ml/kg/hr. Rectal temperature was maintained at 37.5°C. Expired CO_2 was maintained between 4.5%–5.5% by adjusting the stroke volume and ventilation rate of a respiration pump. A broad-spectrum antibiotic (in monkeys, Bicillin, 50,000 i.u./kg, every other day; in cats, Cephazolin, 20 mg/kg i.m., twice daily) and anti-inflammatory steroid (Dexamethasone: in monkeys, 0.5 mg/kg every other day; in cats, 0.4 mg/kg daily). Cats also received an anticholinergic agent (atropine sulfate, 0.05 mg/kg i.m., daily).

Optical Imaging

Imaging of orientation maps in monkeys was performed as described in detail elsewhere (Nauhaus and Ringach, 2007). Briefly, a Dalsa 1M60 camera (Dalsa, Waterloo, Ontario) fitted with a 55 mm telecentric lens (Edmund Optics, NJ) was used for imaging. For illumination we used Illumination Technologies' (East Syracuse, NY) 3900 Smart-Lite illuminator with appropriate focusing filters to achieve an even illumination across the cortical surface. Vasculature images were obtained using a green filter, while intrinsic images were obtained using red illumination and a 700 nm filter with 20 nm bandwidth (Spectra Physics #58460, Mountain View, CA).

Drifting gratings were presented at 8 equally spaced orientations, in both directions (16 conditions). Each condition was presented ~30 times for 3 s, and followed by a 5 s "blank" to bring the hemodynamic signal back to baseline. From these responses we generated an orientation map by computing the resultant of the vector sum of the images (Bonhoeffer and Grinvald, 1991) after appropriate spatial filtering of the images.

Imaging of orientation maps in cats was performed as described in detail elsewhere (Benucci et al., 2007). We stained the cortex with the VSD RH-1692 and imaged its fluorescence. The dye was circulated in a chamber over the cortex for 3 hr and washed out with artificial cerebrospinal fluid. We acquired images with a digital camera (1M60 Dalsa, Waterloo, Ontario), as part of the Imager 3001 setup (Optical Imaging Inc, Rehovot, Israel). Images were acquired at a frame rate of 110 Hz, with spatial resolution of 28 μm per pixel. Additional spatial filtering was performed offline (band-pass, 0.2–2.2 cycles/mm). Frame acquisition was synchronized with the respirator. Illumination from a 100W halogen light was delivered through two optic fibers. The excitation light was band-pass filtered at 630 ± 10 nm, and the emission filter was high pass, with cutoff at 665 nm.

Local Homogeneity Index

Our local homogeneity index resembles the "local input orientation selectivity index" defined by others (Marino et al., 2005; Schummers et al., 2004). Given a map of orientation preferences, the local homogeneity index for a cortical location **x** is defined by the expression:

$$LHI(\mathbf{x}) = \frac{1}{2\pi\sigma^2}\left|\int \exp\left(\frac{-\|\mathbf{x}-\mathbf{y}\|^2}{2\sigma^2}\right)\exp(i2\theta_{\mathbf{y}})d\mathbf{y}\right|$$

Here, $\theta_{\mathbf{y}}$ is the orientation preference at site **y**, and the parameter σ determines the spatial scale of analysis. We used a value of $\sigma = 180$ μm to match the spatial extent of dendritic fields in the superficial layers of cat and monkey.

We also analyzed how the correlation between orientation bandwidth and the homogeneity index was influenced by the selection of spatial scale, σ, used to compute the local homogeneity index. The results (not shown) indicate that the relationship holds up to spatial scales of about 200 μm in the monkey and 300 μm in the cat, degrading rapidly for higher values.

Array Recordings

After the completion of the imaging procedure, we implanted a 10 × 10 electrode array (400 μm separation and 1.5 mm electrode length) in the same patch of cortex. To avoid excessive cortical damage, the arrays were inserted at high speeds (around 8 m/s) using a pneumatic insertion device. Insertion depths were about 0.8–1 mm. While we lack histological confirmation, most of our recordings were likely to originate within the superficial layers of the cortex. The array and surrounding tissue was covered in 1.5% agar to improve stability. After the array was inserted, we took a picture of the array by positioning the camera at about the same location used for the imaging experiments. This picture was later used to establish the search region for the optimal location of the array.

Signals that crossed a specified threshold in each electrode were saved to disk for spike sorting at a later stage. These threshold crossing events are defined as multiunit activity. Spike sorting was performed via clustering in the space of the first three principal component coefficients. Only clusters of spikes that were well segregated from background noise were defined as single units. Details on our spike sorting procedure and the quality of the data are included in the Supplemental Data.

Visual Stimulation and Analysis

Stimuli consisted of a flashed sequence of randomly oriented gratings and spatial phases of fixed spatial frequency. With the monkeys, we used 18 equally spaced orientations and 8 equally spaced spatial phases. Refresh rate was 100 Hz, but orientations were updated every two frames, leading to an effective presentation rate of 50 Hz. With the cats, we used 16 equally spaced orientations and 4 equally spaced spatial phases. In all experiments the stimulus was large enough to cover all the receptive fields of the neurons measured by the array.

The analysis of orientation selectivity consisted of computing the stimulus-triggered spike rate averaged across spatial phases (Ringach et al., 1997). The tuning curve was then defined as the spike rate as a function of orientation at the optimal time delay between stimulus and response. For each tuning curve, we then fitted a Gaussian function with mean θ_0 (the preferred orientation), and standard deviation $\Delta\theta$ (the tuning width). As shown experimentally, this procedure yields estimates of orientation preference and bandwidth that correlate highly with conventional measurements of tuning curves using drifting-grating stimuli in both simple and complex cells (Nishimoto et al., 2005).

Data Selection

All sites with multiunit activity that yielded a tuned response to allow an accurate estimate of preferred orientation were used to align the arrays with the orientation maps. These sites were identified based on the variance of responses across orientation, calculated at different delay times, ranging from 0 to 120 ms. A noise level for the variance was computed at noncausal times (i.e., when the response and the stimulus could not be related one to the other.) If the maximum attained variance within the (0–120 ms) interval was less than twice that of the noise, we discarded the electrode. All other electrodes were considered for the alignment. The first column in Table S1 (available online) lists the number of such sites for each animal. Spike sorting was then performed for all electrodes, irrespective of whether or not they were used in the alignment phase. In the vast majority of cases, however, single units were isolated from those same electrodes that yielded reasonably tuned multiunit activity (95% of the cases in the monkey data and 94% in the cat data). The total number of isolated units obtained in each animal is listed in the second column of Table S1. Orientation tuning curves from individual cells were selected for analysis only if the Gaussian fits accounted for more than 60% of the variance. This was done to exclude single units with noisy tuning curves that could result in inaccurate estimates of preferred orientations and bandwidths. There are various reasons poor tuning could manifest in some cells, but a central one is that the experiments were performed at a fixed spatial frequency that was effective in driving the bulk of the cell population. It is possible that some neurons were not responding robustly due to the use of spatial frequencies that were not within their response range. The numbers of cells that passed the 60% variance criterion in each case and whose location fell within the region of interest of the optical maps are listed in the third column of Table S1. There was no obvious relationship between the cells excluded and their location on the orientation map.

SUPPLEMENTAL DATA

The Supplemental Data for this article can be found online at http://www.neuron.org/cgi/content/full/57/5/673/DC1/.

ACKNOWLEDGMENTS

This work was supported by NIH-EY-17396 (M.C.), EY-12816 (D.L.R.) and EY-18322 (D.L.R.), DARPA FA8650-06-C-7633 (D.L.R.), an Oppenheimer/Stein Endowment Award (D.L.R.), and a Scholar Award from the McKnight Endowment Fund for Neuroscience (M.C.). We are grateful to Robert Frazor, Andy Henrie, and Brian Malone for data collection and valuable discussions.

Received: October 9, 2007
Revised: December 10, 2007
Accepted: January 18, 2008
Published: March 12, 2008

REFERENCES

Alonso, J.M., Usrey, W.M., and Reid, R.C. (2001). Rules of connectivity between geniculate cells and simple cells in cat primary visual cortex. J. Neurosci. *21*, 4002–4015.

Benucci, A., Frazor, R.A., and Carandini, M. (2007). Standing waves and traveling waves distinguish two circuits in visual cortex. Neuron *55*, 103–117.

Blasdel, G.G. (1992). Orientation selectivity, preference, and continuity in monkey striate cortex. J. Neurosci. *12*, 3139–3161.

Blasdel, G.G., and Salama, G. (1986). Voltage-sensitive dyes reveal a modular organization in monkey striate cortex. Nature *321*, 579–585.

Bonhoeffer, T., and Grinvald, A. (1991). Iso-orientation domains in cat visual-cortex are arranged in pinwheel-like patterns. Nature *353*, 429–431.

Bonhoeffer, T., and Grinvald, A. (1993). The layout of iso-orientation domains in area-18 of cat visual-cortex - optical imaging reveals a pinwheel-like organization. J. Neurosci. *13*, 4157–4180.

Callaway, E.M. (1998). Local circuits in primary visual cortex of the macaque monkey. Annu. Rev. Neurosci. *21*, 47–74.

Crair, M.C., Ruthazer, E.S., Gillespie, D.C., and Stryker, M.P. (1997). Relationship between the ocular dominance and orientation maps in visual cortex of monocularly deprived cats. Neuron *19*, 307–318.

Crook, J.M., Eysel, U.T., and Machemer, H.F. (1991). Influence of Gaba-induced remote inactivation on the orientation tuning of cells in area-18 of feline visual-cortex - a comparison with area-17. Neuroscience *40*, 1–12.

De Valois, R.L., Yund, E.W., and Hepler, N. (1982). The orientation and direction selectivity of cells in macaque visual cortex. Vision Res. *22*, 531–544.

Ferster, D., and Miller, K.D. (2000). Neural mechanisms of orientation selectivity in the visual cortex. Annu. Rev. Neurosci. *23*, 441–471.

Gilbert, C.D., and Wiesel, T.N. (1979). Morphology and intra-cortical projections of functionally characterized neurons in the cat visual-cortex. Nature *280*, 120–125.

Grinvald, A., and Hildesheim, R. (2004). VSDI: A new era in functional imaging of cortical dynamics. Nat. Rev. Neurosci. *5*, 874–885.

Hetherington, P.A., and Swindale, N.V. (1999). Receptive field and orientation scatter studied by tetrode recordings in cat area 17. Vis. Neurosci. *16*, 637–652.

Hirsch, J.A. (2003). Synaptic physiology and receptive field structure in the early visual pathway of the cat. Cereb. Cortex *13*, 63–69.

Lund, J.S., and Yoshioka, T. (1991). Local circuit neurons of macaque monkey striate cortex. 3. Neurons of Laminae 4b, 4a, and 3b. J. Comp. Neurol. *311*, 234–258.

Lund, J.S., and Wu, C.Q. (1997). Local circuit neurons of macaque monkey striate cortex. 4. Neurons of laminae 1–3A. J. Comp. Neurol. *384*, 109–126.

Maldonado, P.E., Godecke, I., Gray, C.M., and Bonhoeffer, T. (1997). Orientation selectivity in pinwheel centers in cat striate cortex. Science *276*, 1551–1555.

Marino, J., Schummers, J., Lyon, D.C., Schwabe, L., Beck, O., Wiesing, P., Obermayer, K., and Sur, M. (2005). Invariant computations in local cortical networks with balanced excitation and inhibition. Nat. Neurosci. *8*, 194–201.

McLaughlin, D., Shapley, R., and Shelley, M. (2003). Large-scale modeling of the primary visual cortex: influence of cortical architecture upon neuronal response. J. Physiol. (Paris) *97*, 237–252.

Metin, C., Godement, P., and Imbert, M. (1988). The primary visual cortex in the mouse: receptive field properties and functional organization. Exp. Brain Res. *69*, 594–612.

Nauhaus, I., and Ringach, D.L. (2007). Precise alignment of micromachined electrode arrays with v1 functional maps. J. Neurophysiol. *97*, 3781–3789.

Nishimoto, S., Arai, M., and Ohzawa, I. (2005). Accuracy of subspace mapping of spatiotemporal frequency domain visual receptive fields. J. Neurophysiol. *93*, 3524–3536.

Ohki, K., Chung, S., Ch'ng, Y.H., Kara, P., and Reid, R.C. (2005). Functional imaging with cellular resolution reveals precise micro-architecture in visual cortex. Nature *433*, 597–603.

Ohki, K., Chung, S.Y., Kara, P., Hubener, M., Bonhoeffer, T., and Reid, R.C. (2006). Highly ordered arrangement of single neurons in orientation pinwheels. Nature *442*, 925–928.

Ringach, D.L. (2007). On the origin of the functional architecture of the cortex. PLoS ONE *2*, e251.

Ringach, D.L., Hawken, M.J., and Shapley, R. (1997). Dynamics of orientation tuning in macaque primary visual cortex. Nature *387*, 281–284.

Ringach, D.L., Shapley, R.M., and Hawken, M.J. (2002). Orientation selectivity in macaque V1: Diversity and Laminar dependence. J. Neurosci. *22*, 5639–5651.

Rose, D., and Blakemore, C. (1974). An analysis of orientation selectivity in the cat's visual cortex. Exp. Brain Res. *20*, 1–17.

Schiller, P.H., Finlay, B.L., and Volman, S.F. (1976). Quantitative studies of single-cell properties in monkey striate cortex. II. Orientation specificity and ocular dominance. J. Neurophysiol. *39*, 1320–1333.

Schummers, J., Marino, J., and Sur, M. (2002). Synaptic integration by V1 neurons depends on location within the orientation map. Neuron *36*, 969–978.

Schummers, J., Marino, J., and Sur, M. (2004). Local networks in visual cortex and their influence on neuronal responses and dynamics. J. Physiol. (Paris) *98*, 429–441.

Sompolinsky, H., and Shapley, R. (1997). New perspectives on the mechanisms for orientation selectivity. Curr. Opin. Neurobiol. *7*, 514–522.

Swindale, N.V., Grinvald, A., and Shmuel, A. (2003). The spatial pattern of response magnitude and selectivity for orientation and direction in cat visual cortex. Cereb Cortex. *13*, 225–238.

Van Hooser, S.D., Heimel, J.A.F., Chung, S., Nelson, S.B., and Toth, L.J. (2005). Orientation selectivity without orientation maps in visual cortex of a highly visual mammal. J. Neurosci. *25*, 19–28.

Van Hooser, S.D. (2007). Similarity and diversity in visual cortex: Is there a unifying theory of cortical computation? Neuroscientist *13*, 639–656.